Bistable Prestressed Shell Structures

E. Kebadze[*], S.D. Guest, and S. Pellegrino [†]

Department of Engineering, University of Cambridge

Trumpington Street, Cambridge, CB2 1PZ, UK

Abstract

The paper investigates a cylindrical shell which has two stable configurations, due to a particular distribution of residual stresses induced by plastic bending. The basic mechanics of the bistability are explained, along with details of the plastic forming. A comprehensive analytical model is developed which predicts the residual stress distribution and bistable configurations of the shell. Good correlation has been found between experimental results and predictions from this model.

Keywords: deployable structures, shell structures, prestress, bistable.

[*]Currently at Deep Sea Engineering, London, UK.

[†]Corresponding author, e-mail: pellegrino@eng.cam.ac.uk

Nomenclature

$\mathbf{C}$	material stiffness matrix
$\mathbf{C_t}$	material tangent stiffness matrix
D	plate bending stiffness
E	Young's modulus
E_i	tangent modulus at point i
f	yield function
M_{ix}, M_{iy}	edge bending moments per unit length at step i
t	thickness
U	strain energy per unit area
x, y	longitudinal and transverse coordinates (defined for original configuration)
z	through-thickness coordinate measured from mid plane
z_{cr}	critical depth
α	elastic stress factor
$\boldsymbol{\epsilon}$	vector of principal strain components
ϵ_x, ϵ_y	normal strain components
θ	twist angle
$\boldsymbol{\kappa}$	curvature vector
κ_c	curvature of cylindrical surface
κ_{ix}, κ_{iy}	longitudinal and transverse curvatures at step i
ν	Poisson's ratio
$\boldsymbol{\sigma}$	vector of principal stress components
σ_{ix}, σ_{iy}	normal stress components at step i
σ_M	von Mises effective stress
σ_0	yield stress in pure tension

Subscripts and superscripts:

$(\,)_{cr}$	critical depth
$(\,)_e$	elastic
$(\,)_p$	plastic
$(\,)^y$	non-linear material property
$(\,)', (\,)''$	values at z_{cr} and at surface

Operators:

δ	change between two consecutive sub-increments
Δ	change between two consecutive steps
$(\dot{})$	rate of change

1 Introduction

Bi-stable structures have many applications, the most common being in mechanical and electro-mechanical devices that switch between a discrete number of states. They are also of great interest in the field of deployable structures, where they can be used to develop deceptively simple structures that reliably deploy from their packaged state into their operational configuration.

It is well-known that a thin elastic shell in the form of a portion of a cylindrical surface, of arbitrary length, radius, and cross-sectional angle can be flattened at one end and rolled up. This is the working principle of the steel tape measure, which typically has cross-sectional angles of 50-70°, and also of the storable tubular extendible member (Rimrott 1965) and a family of related structures (MacNaughton, Weyman, and Groskopfs 1967) with cross-sectional angles up to 400°. Although the deformation of these shells is essentially inextensional, as both the extended and coiled configurations are cylindrical and hence there is no change in the product of the two principal curvatures, or gaussian curvature (Calladine 1983), there is still a significant amount of bending strain energy in the coiled configuration. These coiled shells are not in equilibrium without the application of external forces, and hence a containment mechanism is required. An example is shown in Figure 1.

There are two different ways of making the coiled configuration of these cylindrical shells stable, so that the containment mechanism becomes unnecessary. The first approach, first exploited by Daton-Lovatt (1996) in the design of composite booms able to carry heavy inspection devices in nuclear reactors, makes use of special lay-ups of the composite. It has been investigated by Iqbal and Pellegrino (2000), Iqbal, Pellegrino and Daton-Lovatt (2000), and Galletly and Guest (2003a, 2003b). In this approach the non-zero curvatures, transverse in the extended configuration and longitudinal in the coiled configuration, have equal signs —as in the tape measure of Figure 1. Several studies of related bi-stable composite structures have been made by Hyer (1981a, 1981b).

The second approach, which is the object of this paper, is complementary to the first, and leads to the two curvatures being of opposite sign. Figure 2 shows the *steel* tape that is found inside the bright fabric cover of a "slap bracelet" that can be found in many toy stores. Figures 2(a) and 2(e) show the two stable configurations. Configuration (a) represents a high energy state; if one flattens any cross section,

the structure jumps to the configuration (e). If one flattens both end cross sections and holds the ends allowing two separate coils to form and gradually move towards one another, then the intermediate configurations (b-d) are observed. Between the configuration in Figure 2(c) and Figure 2(d) there is a sudden snap as the central part of the shell "pops up".

This paper explains why this particular tape behaves as it does, and describes a forming process that leads to this behaviour. An analytical model of this elasto-plastic forming process is then introduced, based on the assumption that the shell is uniformly curved, from which quantitative predictions can be made. Predictions for Beryllium-Copper tapes with different radii of curvatures are made and compared with experimental measurements; they are found to be in good agreement.

The layout of the paper is as follows. Section 2 presents some initial experimental observations. Section 3 describes the elasto-plastic forming process of a thin metallic strip that leads to a distribution of residual stresses that cause bi-stable behaviour. The associated stress distributions are analysed, assuming a rigid-perfectly plastic material model, and analytical expressions for the distribution of residual stresses and curvatures of the strip in the two equilibrium configurations are obtained. Section 4 presents a more realistic, iterative technique for simulating the forming process, leading to a more refined estimate of the stresses and curvatures. Sections 5 and 6 compare the results from this model to measurements obtained from six experiments. Section 7 investigates the stability of equilibrium configurations identified in the earlier part of the study. Section 8 discusses the results obtained and concludes the paper.

2 Two Physical Models

Since it is unusual for a shell structure to behave in the way shown in Figure 2, it seems obvious to investigate if some initial stresses in the shell might be the cause of this behaviour. Hence, the steel tape was sliced up longitudinally and transversally, and the strips that were obtained are shown in Figure 3. It can be seen that the longitudinal strips are curved upwards, whereas the transverse strips are curved downwards and have a curvature matching the transverse curvature of the shell in the extended configuration. Clearly the tape is subject to initial bending stresses.

If the tape is held completely flat, the longitudinal and transverse stresses tend to bend it in opposite directions.

A simple, related bi-stable structure can be made from half-circular strips made from Beryllium-Copper, as follows. Figure 4(a) shows 12 identical strips, divided into two parallel sets, one curved upwards and one downwards. In Figure 4(b) the two sets of strips are held straight in a wooden frame and have been spot-welded at each intersection point. When this structure is removed from the frame, it is found to be bi-stable, and Figures 4(c-d) show its two stable configurations. Note that, due to the plastic deformation that occurs during welding, the curvatures in the two configurations are smaller than in the original strips.

3 Forming Process and Residual Stresses

The simplest way of inducing residual stresses in a homogeneous, isotropic shell is by deforming it beyond its yield point. This section describes the various steps of the forming process, and explains how the associated stress distribution can be achieved, assuming a simple elastic-perfectly plastic material model. A more accurate analysis of the stress state is then presented in Section 4.

Figure 5 shows the two stable configurations of a shell made by heat-treating a thin, square sheet of Beryllium-Copper and then plastically bending it as described next. This shell is initially manufactured by placing a flat sheet of soft, annealed Beryllium-Copper in a cylindrical former, where it is age-hardened by suitable heat treatment. Figure 6 shows the cylindrical shell that is thus obtained; this initial configuration is assumed to be unstressed.

A curvilinear coordinate system will be used throughout this paper. The x and y-directions are defined to be parallel to the cylindrical and circumferential axes, respectively, when the shell is in its initial configuration and the z-coordinate is perpendicular to the cylindrical surface. The x and y-directions will be principal directions of curvature throughout, and it will be also assumed that the curvature of the shell is uniform. For clarity, in Figure 6 and subsequent figures we have shown the orientation of the shell by drawing the tangent vectors to the x and y-directions at a point on the centre line. Note that, because of the uniform curvature assumption, there is no need to choose a specific origin for the coordinate system.

Our sign convention for curvature is defined in Figure 6 and the sign convention for moments follows from it, i.e. positive moments apply positive curvatures. Note that the principal, initial curvatures are $\kappa_{0x} = 0$ and $\kappa_{0y} > 0$.

The cylindrical Beryllium-Copper shell obtained as described above is then put through a series of uniform curvature changes that leave behind a set of residual stresses that make it bi-stable. Note that in the curvature changes that are described, stretching of the mid-surface of the shell is always avoided by going through a flat, intermediate configuration instead of going directly from one curved configuration to another.

The first step in the forming process consists in flattening the shell by applying edge bending moments per unit length M_{1x} and M_{1y} such that $\kappa_{1x} = \kappa_{1y} = 0$, Figure 7(a). Assuming that the shell remains in the elastic range during this deformation, the stress distribution through the thickness is linear, as shown in Figure 7(b). The stress σ_{1y} is the direct result of the imposed change of curvature in the y-direction, whereas the stress σ_{1x} is due to Poisson's ratio effects; these stresses are determined by:

$$\sigma_{1x} = -\frac{\nu E}{1-\nu^2} z \kappa_{0y} \tag{1}$$

$$\sigma_{1y} = -\frac{E}{1-\nu^2} z \kappa_{0y} \tag{2}$$

where z is the distance from the mid-surface of the shell; E is the Young's Modulus and ν the Poisson's ratio of the material. Equations 1-2 are valid for *thin shells*, where the product of thickness by curvature is small; this assumption is carried through the rest of the derivation. In the present study, the largest value of this product is 3%.

In the second step, the bending moment M_x is further increased in magnitude until κ_x reaches the value κ_{2x} (< 0), see Figure 8(a). During this process the transverse curvature κ_y is kept constant, hence $\kappa_{2y} = 0$. However, no edge bending moment M_y needs to be applied because membrane stresses equivalent to the resultant of the required M_{2y} are set up in the shell, see Figure 9. The magnitude of these membrane stresses is negligible in comparison with the bending stresses, and hence they will be neglected. Right on the edge, the shell will maintain its original curvature κ_{0y} and hence a small boundary layer will form; this effect will be neglected for simplicity.

The magnitude of κ_{2x} is such that plastic deformation occurs for $|z| > z_{cr}$. In order to find z_{cr} the central portion of the shell, $|z| < z_{cr}$, is assumed to behave elastically and hence the stress distribution is linear, as shown in Figure 8(b), and is determined by:

$$\sigma_{2x} = \frac{E}{1-\nu^2}\, z\,(\kappa_{2x} - \nu\kappa_{0y}) \tag{3}$$

$$\sigma_{2y} = \frac{E}{1-\nu^2}\, z\,(\nu\kappa_{2x} - \kappa_{0y}) \tag{4}$$

The critical depth z_{cr} can be determined using the von Mises yield criterion for plane stress

$$\sigma_x^2 - \sigma_x\sigma_y + \sigma_y^2 = \sigma_0^2 \tag{5}$$

where σ_0 is the yield stress in simple tension, and Equations (3) and (4) can be substituted for σ_x and σ_y. Hence, solving for z

$$z_{cr} = \frac{(1-\nu^2)\sigma_0}{E\sqrt{(1-\nu^2)(\kappa_{0y}+\kappa_{2x})^2 + (\nu\,\kappa_{0y} - \kappa_{2x})(\kappa_{0y} - \nu\,\kappa_{2x})}} \tag{6}$$

Between $+z_{cr}$ and $-z_{cr}$ the material behaves elastically. Beyond these limits the stress distribution depends on the plastic properties of the material, i.e. its hardening characteristics. Even for an elastic-perfectly plastic material it is impossible to find the exact stresses after yield without a detailed, iterative calculation. This is because of the interaction between elastic and plastic deformation, and the two-dimensional nature of the present situation.

Figure 10(a) shows the yield locus for a von Mises material in plane stress,and the stress trajectory for a point on the bottom surface of the shell, as we go through the first two steps.

Figure 10(b) shows the strain trajectory for the same point. As the shell is flattened in Step 1, $\varepsilon_x = 0$ and $\varepsilon_y > 0$, hence in Figure 10(b) the strain goes from O to A and the stresses change accordingly, see Figure 10(a). The slope of the line OA in stress space depends on the Poisson's ratio of the material.

During Step 2 only κ_x and ε_x change. In stress space the corresponding line ABD has a different slope from OA. If the shell was completely elastic the stresses would go to point D, but at point B yielding begins and hence the stress trajectory has to follow the yield locus to point C. Meanwhile, in strain space —Figure 10(b)— the total strain trajectory is in the same direction as before, as κ_y and hence ε_y continue to be zero, but now each strain increment consists of two components: elastic, $\boldsymbol{\varepsilon}_e$,

and plastic, $\boldsymbol{\varepsilon}_p$. The elastic strain component brings the stresses to point C, on the yield locus, and the plastic strain is such that the *total strain* is an increment purely in ε_x, thus leading to point C$'$ in Figure 10(b).

The location of point C depends on how far D is from B. If they coincide, then the material has just yielded and there is no movement on the locus and so $\boldsymbol{\varepsilon}_p = 0$. If D was very far from B, then $||\boldsymbol{\varepsilon}_p|| >> ||\boldsymbol{\varepsilon}_e||$ and so, assuming $\boldsymbol{\varepsilon}_e \approx 0$, the total strain increment has to satisfy the plastic flow rule (Lubliner 1990). Hence, since the strain increment involves only ε_x, the stresses would have to correspond to point G.

In this particular case, though, $\boldsymbol{\varepsilon}_e$ and $\boldsymbol{\varepsilon}_p$ are of the same order, and so the stresses will be on the locus somewhere between points B and G. The exact location can only be found through a proper elasto-plastic iteration but the result is schematically shown by the zig-zag line in Figure 10(b). A proper iterative solution will be described in the next section.

Having shown that the exact stresses beyond z_{cr} cannot be found in a simple way, we will make a crude simplifying assumption that enables us to complete this preliminary analysis. We will assume that the stresses in the plastic region are *uniform*. The corresponding stress distribution, shown in Figure 8(b) with a solid line, is fully determined by z_{cr} and by

$$\sigma'_{2x} = \sigma''_{2x} = \frac{E}{1-\nu^2}\, z_{cr}\, (\kappa_{2x} - \nu\kappa_{0y}) \tag{7}$$

$$\sigma'_{2y} = \sigma''_{2y} = \frac{E}{1-\nu^2}\, z_{cr}\, (\nu\kappa_{2x} - \kappa_{0y}) \tag{8}$$

In Step 3 the moment M_{2x} is removed from the shell. This unloading is assumed here elastic, and leaves the shell with a residual curvature $\kappa_{3x}\,(< 0)$, as shown in Figure 11(b). The stress increments from the end of step 2 are due to the curvatures changes $\kappa_{3x} - \kappa_{2x}$ only, as $\kappa_{3y} = \kappa_{2y} = 0$. Therefore

$$\sigma'_{3x} = \sigma'_{2x} + \frac{E}{1-\nu^2}\, z_{cr}\, (\kappa_{3x} - \kappa_{2x}) \tag{9}$$

$$\sigma'_{3y} = \sigma'_{2y} + \frac{E}{1-\nu^2}\, z_{cr}\, \nu(\kappa_{3x} - \kappa_{2x}) \tag{10}$$

$$\sigma''_{3x} = \sigma''_{2x} + \frac{E}{1-\nu^2}\, \frac{t}{2}\, (\kappa_{3x} - \kappa_{2x}) \tag{11}$$

$$\sigma''_{3y} = \sigma''_{2y} + \frac{E}{1-\nu^2}\, \frac{t}{2}\, \nu(\kappa_{3x} - \kappa_{2x}) \tag{12}$$

The configuration of the shell at the end of step 3 is determined by the requirement that the residual stresses σ_x in this configuration have zero resultant moment.

Integrating $\sigma_x\, z$ gives

$$M_{3x} = 2\left[\frac{1}{3}\sigma'_{3x}\, z_{cr}^2 + \frac{\sigma'_{3x}+\sigma''_{3x}}{2}\left(\frac{t}{2}-z_{cr}\right)\left(z_{cr}+\frac{\frac{t}{2}-z_{cr}}{3}\frac{\sigma'_{3x}+2\,\sigma''_{3x}}{\sigma'_{3x}+\sigma''_{3x}}\right)\right] \tag{13}$$

Setting $M_{3x}=0$ and substituting Equations(3, 10, 11), gives an equation that can be solved for κ_{3x} to obtain

$$\kappa_{3x} = \frac{z_{cr}}{t^3}\left(4\, z_{cr}^2 - 3\, t^2\right)\left(\kappa_{2x} - \nu\,\kappa_{0y}\right) + \kappa_{2x} \tag{14}$$

Note that κ_{3x} is a function of the initial curvature κ_{0y}, the applied curvature κ_{2x}, and of the yield stress of the material, through z_{cr}. At this curvature the stresses σ_y have non-zero resultant, but are equilibrated by membrane stresses, as shown in Figure 9.

The plastic forming process is now complete, and the shell is in one of its two stable states. Steps 4 and 5 now elastically transform the structure to its other stable state. In practice, see Section 5, this transformation may involve further plastic deformation, but this is not considered here, for simplicity.

In step 4, the shell is flattened again, Figure 12, by applying the edge moments M_{4x} and M_{4y}. Figure 12(b) shows the stress distribution through the shell; the salient points can be determined from σ'_{2x} and σ'_{2y}, by considering directly the elastic stress changes from step 2.

If now, step 5, the edge moment M_{4y} is removed, the shell bends into the shape shown in Figure 13(a) and the moment M_{4x} can then be removed without causing any significant deformation in the x-direction. In analogy with step 3, the removal of M_{4x} results in purely membrane stresses. The shell is deformed until the bending moment resulting from σ_y is zero, and this determines the value of the curvature κ_{5y}. Again, a purely linear-elastic response is assumed and hence the salient stress values corresponding to the curvatures κ_{5x} $(=0)$ and κ_{5y} are

$$\sigma'_{5x} = \sigma'_{2x} + \frac{E}{1-\nu^2}\, z_{cr}(\nu\kappa_{5y} - \kappa_{2x}) \tag{15}$$

$$\sigma'_{5y} = \sigma'_{2y} + \frac{E}{1-\nu^2}\, z_{cr}(\kappa_{5y} - \nu\kappa_{2x}) \tag{16}$$

$$\sigma''_{5x} = \sigma'_{2x} + \frac{E}{1-\nu^2}\,\frac{t}{2}(\nu\kappa_{5y} - \kappa_{2x}) \tag{17}$$

$$\sigma''_{5y} = \sigma'_{2y} + \frac{E}{1-\nu^2}\,\frac{t}{2}(\kappa_{5y} - \nu\kappa_{2x}) \tag{18}$$

The residual curvature κ_{5y} can be found, as before, by setting the moment of the stresses σ_y equal to zero. This gives

$$\kappa_{5y} = \frac{z_{cr}}{t^3}\left(4\, z_{cr}^2 - 3\, t^2\right)\left(\nu\,\kappa_{2x} - \kappa_{0y}\right) + \nu\,\kappa_{2x} \tag{19}$$

The two stable configurations of the structure in Figure 5 correspond to the curvatures κ_{3x} and κ_{5y}. Note that their analytical expressions, given by Equations (14) and (19), are similar, apart from swapping the terms multiplied by the Poisson's ratio.

4 Modelling the Forming Process

The simple model of the forming process described in the previous section is unable to capture the actual behaviour of high yield strain, strain-hardening materials, and hence gives rather poor agreement with experiments. To obtain reasonable predictions a more refined model is required, involving an iterative analysis, and this will be presented next.

The simulation of the forming process follows the same sequence of deformation that was described in the previous section. Again, the bending curvatures are assumed to be uniform throughout the shell, hence only an element of shell of unit dimensions needs to be analysed, and stretching of the mid-surface is ignored. Plane sections are assumed to remain plane.

An isotropic strain hardening material model is assumed; this is the simplest model that captures the behaviour observed experimentally. Readers are referred to textbooks such as Lubliner (1990) for an introduction to this model and to Crisfield (1991) for details on the computational formulation adopted here. A brief review of the computational procedure is given next.

Figure 14 shows the stress-strain relationship for the age-hardened Beryllium-Copper used in our experiments, obtained experimentally from a uniaxial test in tension. This curve can be approximated as piece-wise linear; the corresponding pairs of stress/strain values are listed in Table 1.

After first yield, the plastic strain at point i is determined by:

$$\varepsilon_{p_i} = \varepsilon_i^y - \frac{\sigma_i^y}{E} \tag{20}$$

To model strain hardening, the quantity $\partial\sigma^y/\partial\varepsilon_p$ is required. This can be obtained from

$$H_i = \frac{\partial\sigma^y}{\partial\varepsilon_p} = \frac{E_i}{1 - E_i/E} \tag{21}$$

where E_i is the tangent modulus, i.e.

$$E_i = \frac{\sigma_i^y - \sigma_{i-1}^y}{\varepsilon_i^y - \varepsilon_{i-1}^y} \tag{22}$$

Assuming that the shell is in a state of plane stress, at a general point the principal stress components are defined by the stress vector

$$\boldsymbol{\sigma} = \begin{bmatrix} \sigma_x \\ \sigma_y \end{bmatrix}$$

and the principal strains by the strain vector

$$\boldsymbol{\varepsilon} = \begin{bmatrix} \varepsilon_x \\ \varepsilon_y \end{bmatrix}$$

The von Mises effective stress is

$$\sigma_M = \frac{1}{\sqrt{2}} \sqrt{\boldsymbol{\sigma}^{\mathrm{T}} \mathbf{A}\, \boldsymbol{\sigma}} \tag{23}$$

where

$$\mathbf{A} = \begin{bmatrix} 2 & -1 \\ -1 & 2 \end{bmatrix}$$

and hence the yield condition can be written in the form

$$f = \sigma_M - \sigma_0^y = \frac{1}{\sqrt{2}} \sqrt{\boldsymbol{\sigma}^{\mathrm{T}} \mathbf{A}\, \boldsymbol{\sigma}} - \sigma_0^y \leq 0 \tag{24}$$

Before the material yields, $\boldsymbol{\sigma}$ and $\boldsymbol{\varepsilon}$ are related by $\boldsymbol{\sigma} = \mathbf{C}\boldsymbol{\varepsilon}$, where $\mathbf{C}$ is the material stiffness matrix

$$\mathbf{C} = \frac{E}{1-\nu} \begin{bmatrix} 1 & \nu \\ \nu & 1 \end{bmatrix}$$

After the material has yielded the effective plastic strain rate is

$$\dot{\varepsilon}_p = \frac{2}{\sqrt{3}} \left(\dot{\varepsilon}_{px}^2 + \dot{\varepsilon}_{py}^2 + \dot{\varepsilon}_{px} \dot{\varepsilon}_{py} \right) \tag{25}$$

and hence the effective plastic strain is

$$\varepsilon_p = \int \dot{\varepsilon}_p \tag{26}$$

The relationship between $\dot{\boldsymbol{\sigma}}$ and $\dot{\boldsymbol{\varepsilon}}$ is given by the tangent material stiffness matrix $\mathbf{C}_t$, where

$$\mathbf{C}_{\mathrm{t}} = \mathbf{C} \left(\mathbf{I} - \frac{\mathbf{a}\, \mathbf{a}^{\mathrm{T}}\, \mathbf{C}}{\mathbf{a}^{\mathrm{T}}\, \mathbf{C}\, \mathbf{a} + H} \right) \tag{27}$$

Here $\mathbf{I}$ is a 2×2 identity matrix, $\mathbf{a}$ the normal to the yield surface

$$\mathbf{a} = \frac{\mathbf{A}\,\boldsymbol{\sigma}}{2\,\sigma_M} \tag{28}$$

and the hardening parameter H depends the current plastic strain.

The first step in modelling the forming process consists in computing the curvature changes associated with Steps 1-5 described in Section 3. The corresponding changes in the curvature vectors are:

$$\Delta\boldsymbol{\kappa}_1 = \begin{bmatrix} 0 \\ -\kappa_{0y} \end{bmatrix};\ \Delta\boldsymbol{\kappa}_2 = \begin{bmatrix} \kappa_{2x} \\ 0 \end{bmatrix};\ \Delta\boldsymbol{\kappa}_3 = \begin{bmatrix} \kappa_{3x} - \kappa_{2x} \\ 0 \end{bmatrix};\ \Delta\boldsymbol{\kappa}_4 = \begin{bmatrix} -\kappa_{3x} \\ 0 \end{bmatrix};\ \Delta\boldsymbol{\kappa}_5 = \begin{bmatrix} 0 \\ \kappa_{5y} \end{bmatrix}$$

Each curvature change is divided into a series of small sub-increments, which will be denoted by δ. The shell is divided into a series of uniformly stressed thin layers, and the bending moments caused by any given stress distribution are determined at each increment. When the bending moment in the direction in which the shell is curved becomes zero, the shell is in equilibrium and this condition determines the unknown curvatures κ_{3x} and κ_{5y}.

For each curvature increment the following calculations are carried out for each layer, using Matlab (The Mathworks 2002):

1. The elastic stress increment corresponding to the prescribed curvature increment is determined using the material stiffness matrix:

$$\Delta\boldsymbol{\sigma} = \mathbf{C}\,\Delta\boldsymbol{\varepsilon} \tag{29}$$

   where $\Delta\boldsymbol{\varepsilon} = z\,\Delta\boldsymbol{\kappa}$.

2. This elastic stress increment is then checked against the yield condition. Denoting by $\boldsymbol{\sigma}_0$ the stress at the end of the previous increment, if

$$f(\boldsymbol{\sigma}_0 + \Delta\boldsymbol{\sigma}) \leq 0 \tag{30}$$

   then the current increment is completely elastic, and the stress at the end of the increment is $\boldsymbol{\sigma}_1 = \boldsymbol{\sigma}_0 + \Delta\boldsymbol{\sigma}$.

3. If Equation (30) is not satisfied then, in general, the increment involves a purely elastic part, followed by an elasto-plastic part.

   (i) If the stress at the end of the previous increment was *inside* the yield locus, i.e. $f(\boldsymbol{\sigma}_0) < 0$, then the intersection with the yield surface is determined from

$$f(\boldsymbol{\sigma}_0 + \alpha\,\Delta\boldsymbol{\sigma}) = 0 \tag{31}$$

whose solution is

$$\alpha = \frac{\sqrt{\left(\boldsymbol{\sigma}_0^{\mathrm{T}}\,\mathbf{A}\,\Delta\boldsymbol{\sigma}\right)^2 - \left(\Delta\boldsymbol{\sigma}^{\mathrm{T}}\,\mathbf{A}\,\Delta\boldsymbol{\sigma}\right)\left(\boldsymbol{\sigma}_0^{\mathrm{T}}\,\mathbf{A}\,\boldsymbol{\sigma}_0 - 2\left(\sigma^y\right)^2\right)} - \boldsymbol{\sigma}_0^{\mathrm{T}}\,\mathbf{A}\,\Delta\boldsymbol{\sigma}}{\Delta\boldsymbol{\sigma}^{\mathrm{T}}\,\mathbf{A}\,\Delta\boldsymbol{\sigma}} \tag{32}$$

Hence, the stress due to the first part of the increment is $\boldsymbol{\sigma}_1 = \boldsymbol{\sigma}_0 + \alpha\,\Delta\boldsymbol{\sigma}$.

(ii) If the stress at the end of the previous increment was already on the yield locus, i.e. $f(\boldsymbol{\sigma}_0) = 0$, it can be assumed that $\alpha = 0$ and $\boldsymbol{\sigma}_1 = \boldsymbol{\sigma}_0$.

4. The remaining, elasto-plastic part of the increment is divided into m sub-increments:

$$\delta\boldsymbol{\varepsilon} = \frac{1-\alpha}{m}\Delta\boldsymbol{\varepsilon} \tag{33}$$

5. Each corresponding stress sub-increment is calculated using the tangent elasto-plastic matrix $\mathbf{C}_{\mathrm{t}}$ determined at the end of the previous sub-increment, hence

$$\delta\boldsymbol{\sigma} = \mathbf{C}_{\mathrm{t}}\,\delta\boldsymbol{\varepsilon} \tag{34}$$

and the stress at the end of the sub-increment is

$$\boldsymbol{\sigma}_i = \boldsymbol{\sigma}_{i-1} + \delta\boldsymbol{\sigma} \tag{35}$$

This calculation is repeated m times.

Modelling the unloading of the shell when it is flattened and flipped back from step 3 to steps 4 and 5, requires reverse plasticity and the Bauschinger effect to be modelled. Several ways of doing this were explored, but the most accurate results were obtained by abandoning the isotropic hardening model described above when unloading begins. Instead, a kinematic hardening model (Lubliner 1990) is adopted. This involves translating the *original* yield locus by an amount equal to the plastic strain that was accumulated during the previous yielding phase, until the material begins to yield in the reverse direction. At this point, isotropic hardening is re-started and so the yield locus begins to grow again.

This is illustrated in Figure 15. During step 2 the yield locus expands from first yield, at point B, to the beginning of unloading at point C. During step 3 the material unloads linearly from point C to D. At point D reverse yielding begins — note that the yield locus is obtained by translating the original locus by HC— and the yield locus starts expanding again. Point E corresponds to the configuration in which the bending moment M_{3x} is zero. Point F corresponds to the flattened

configuration, and point G to the final, flipped configuration. Section 6 presents detailed results obtained from this model for some particular cases that were also modelled experimentally.

5 Experiments

Six test specimens were made by heat treatment of 0.1 mm thick strip of annealed Beryllium-Copper. The treatment consisted in putting the strip into a cylindrical mould which was then put into a furnace at 316°C for 3.5 hours. This has the effect of age-hardening the material, which sets the strip into a curved shape and increases its yield stress. The uniaxial stress-strain relationship after heat treatment was measured for each strip, see Table 1 and Figure 14, and the curvature of each strip was also measured, see Table 2.

A rolling machine was made, consisting of two identical rollers with radius of 7.5 mm and a removable, upper forming roller with radius of either 3.2 or 4.0 mm; these three rollers are driven by a single handle, through a set of gears. This machine was used to apply the curvature $\kappa_{2x} = 1/3.2$ mm^{-1} or $\kappa_{2x} = 1/4.0$ mm^{-1}.

For each specimen, the residual curvature κ_{3x} was measured after each specimen came out of the rolling machine and the after flipping it over twice. The second flip would return the specimen to κ_{3x} if no further plastic deformation occurs, however there is indeed some further deformation and so the measured values are denoted by κ'_{3x}. The results are listed in Table 3.

Note that much of the deformation imposed by the forming roller is in fact elastic, and hence is lost when the specimens come out of the former, i.e. they go from κ_{2x} to κ_{3x}. Also note that in all cases $\kappa_{3x} \approx \kappa'_{3x}$, which indicates that only a small amount of plastic deformation takes place when the shell is flipped over for the second time. In all six cases it was observed that no further plastic deformation occurs after the second flip.

6 Theoretical Predictions

The forming of each specimen was simulated with Matlab and the predicted residual curvatures are listed in Table 3. Typically, the elasto-plastic stresses were calculated at a minimum of 100 points, uniformly spaced through the thickness.

The first residual curvature, κ_{3x}, just after yielding, is predicted quite accurately in most cases; the largest error is $\approx 30\%$ in test case 2, but in all other cases the error is 20% or less, which confirms that the elasto-plastic behaviour has been captured quite accurately. In general, the predictions for the residual curvatures after flipping, κ_{5y} and κ'_{3x}, are very accurate; there is only one case where there is a large error, of 50% for κ_{5y} in test case 3. These errors may be due to some anomaly during the forming process.

The predicted stress distribution in test case 3, after flipping the shell back to the curvature κ'_{3x} is shown in Figure 16. Note that the general shape of these plots resembles Figures 11(b) and 13(b), but the stress variation through the thickness is now much smoother as the elastic-perfectly plastic transition in the simplified stress-strain relationship that had been assumed in Section 3 has now been replaced with a gradual strain-hardening. The bending moment due to the σ_x distribution is zero, as expected; the moment due to σ_y is -0.52 Nmm/mm.

According to the predictions, which are confirmed experimentally, flipping the shell back and forth after completing the forming process is entirely within the elastic range. Therefore, any further calculation on these shells can be done more conveniently using these residual moments, i.e. without considering the actual, and rather complex stress distributions. This last observation will be exploited in calculating the variation in the strain energy of the shell, in the next section.

7 Stability Considerations

So far, we have considered only equilibrium conditions of a prestressed shell, but it cannot be taken for granted that the two configurations where the shell is in equilibrium will be stable. A fully general stability analysis would be beyond the scope of the present study, but if we consider only deformations of the shell that are *uniform and inextensional* it becomes possible to derive a simple expression of the strain energy from which we can establish if the equilibrium configurations that we have identified are also stable; further details are provided in Guest and Pellegrino (2003). Through this process we will also understand some more general aspects of the bi-stable behaviour of the shell.

For all uniform inextensional deformations the mid-surface of a cylindrical shell

will lie on a cylindrical surface; let the radius of this cylinder be $1/\kappa_c$. Different amounts of twist can be imparted by rotating the shell with respect to the axis of the cylinder, as shown in Figure 17. The angle between the global X-axis on the cylinder and the local x-axis on the shell is denoted by θ, as shown.

Consider a cylindrical shell with initial curvature κ_{0c} in the x-direction. In this initial configuration the shell is not stress free, but is subject to uniform initial stresses σ_y which have resultant bending moment per unit length M_{0y}. This resultant moment is equilibrated by (small) membrane stresses acting in the y-direction and hence the shell is in equilibrium in this configuration.

Now consider an alternative configuration of this shell, obtained by changing the radius of the underlying cylinder to κ_c and by imposing a twist θ. The corresponding changes in curvatures and twist in the local coordinate system x, y can then be obtained by transforming the curvatures expressed in the global coordinate system X, Y to x, y (Timoshenko and Woinowsky-Krieger 1959, Calladine 1983) which gives

$$\begin{aligned} \Delta\kappa_x &= \frac{\kappa_c}{2}(1+\cos 2\theta) - \kappa_{0c} \\ \Delta\kappa_y &= \frac{\kappa_c}{2}(1-\cos 2\theta) \\ \Delta\kappa_{xy} &= -\frac{\kappa_c}{2}\sin 2\theta \end{aligned} \tag{36}$$

This assumes the definition $\kappa_{xy} = -\partial^2 w/\partial x \partial y$ for the twisting curvature, as is standard in the plates and shells literature (but not in the composites literature, where usually $\kappa_{xy} = -2\partial^2 w/\partial x \partial y$).

The strain energy in this new configuration can be readily estimated if edge effects are neglected, i.e. if one assumes —as throughout this paper— that $\Delta\kappa_x$, $\Delta\kappa_y$, and $\Delta\kappa_{xy}$ are uniform throughout the structure. The strain energy per unit area of a shell that is subject to elastic curvatures $\kappa_x, \kappa_y, \kappa_{xy}$ but no mid-surface strains has the expression

$$U = \frac{1}{2}\begin{bmatrix} M_x & M_y & M_{xy} \end{bmatrix} \begin{bmatrix} 1 & 0 & 0 \\ 0 & 1 & 0 \\ 0 & 0 & 2 \end{bmatrix} \begin{bmatrix} \kappa_x \\ \kappa_y \\ \kappa_{xy} \end{bmatrix} \tag{37}$$

Equivalent expressions can be obtained by expressing the curvatures in terms of moments, or the moments in terms of curvatures.

In the present case the total strain energy per unit area can be conveniently written as the sum of three terms, as follows.

1. Strain energy in the initial configuration, i.e. associated with the initial bending moment M_{0y}, given by:

$$U_1 = \frac{1}{2}\frac{{M_{0y}}^2}{D(1-\nu^2)} \tag{38}$$

where $D = \dfrac{E\,t^3}{12(1-\nu^2)}$ is the shell bending stiffness.

2. Work done by the initial bending moment, M_{0y}, for the corresponding curvature change $\Delta\kappa_y$:

$$U_2 = M_{0y}\,\Delta\kappa_y \tag{39}$$

3. Strain energy due to the curvature changes $\Delta\kappa_x, \Delta\kappa_y, \Delta\kappa_{xy}$

$$U_3 = \frac{1}{2}D({\Delta\kappa_x}^2 + 2\nu\,\Delta\kappa_x\,\Delta\kappa_y + {\Delta\kappa_y}^2 + 2(1-\nu)\,\Delta\kappa_{xy}^2) \tag{40}$$

Hence, an expression for the total strain energy is obtained by substituting Equations 38-40 into

$$U = U_1 + U_2 + U_3 \tag{41}$$

and then replacing the curvature changes with the expressions given in Equation 36.

A search for local minima in the energy surface can be carried out by plotting the variation of U with respect to κ_c and θ, which is easily done using a polar contour plot. Figure 18 shows this plot for experimental test case 3, where the initial configuration has $\kappa_x = \kappa'_{3x} = -1/15$ mm and $M_y = -0.52$ Nmm/mm . Note that 2θ has been plotted, instead of θ, so that each configuration is considered only once. The curvature of the cylinder is plotted on the polar axis, however positive and negative curvatures cannot be shown in the same plot, hence negative curvatures have been shown in Figure 18(a), and positive curvatures in Figure 18(b). In each plot there is one energy minimum, note that the two minima are at $2\theta = 180^\circ$ from one another, and hence correspond to a 90° flip of the shell.

Note that the energy minimum in Figure 18(a) has a value lower than the minimum in Figure 18(b), and hence if the shell is in the higher energy stable configuration, a relatively small perturbation would be required to trigger a "jump" to the lower energy configuration. Also note that the curvatures corresponding to these energy minima coincide exactly with those obtained through the equilibrium approach, in Section 6. This is no surprise, of course, because the initial strain energy in the two analyses has been set equal by using M_{0y} to set up the initial strain energy.

Finally, note that the shell cannot lose its stability through twisting because its strain energy increases for any (small) deformation of the shell away from either local minimum.

8 Discussion and Conclusion

The bi-stability of thin, prestressed cylindrical shell structures, whose stable configurations have curvatures of opposite sign, has been explained and analysed in detail. The key effect is that a set of residual bending stresses (i.e. non-uniform through the thickness) acting along the direction of the cylindrical axis needs to be introduced. In the original configuration, these stresses are equilibrated by membrane stresses (i.e. uniform through the thickness) in the shell acting as a beam.

If a sufficiently large disturbance is applied, the shell flips to its alternate stable state in which, again, bending stresses in the now longitudinal direction are equilibrated by membrane stresses. In both configurations, the bending stresses in the transverse direction have zero resultant.

A qualitative analysis of the elastic-plastic forming process that sets up an appropriate distribution of residual stresses has been presented, and a more refined elastic-plastic model with strain hardening has been implemented, based on a uniaxial stress-strain relationship for the material. Using this model, the curvatures of six Beryllium-Copper cylindrical shells that undergo a specified forming process have been estimated, and these estimates have been compared to actual measurements. The errors in the predictions are typically less than 10%.

It is clear that the sequence of uniform curvature states assumed for the model presented in this paper implicitly require the presence of non-zero bending moments along the edges. However, since these edge moments are certainly zero in the final stable states, the predicted stress distributions will be incorrect in a short boundary layer around the edges of the shells. Typically, the length of this boundary layer is the geometric mean of the thickness times the radius of curvature of the shell (Calladine 1983); effects of this type have been studied by Galletly and Guest (2003b).

There are other effects that, although potentially important, were not included in our model. Probably the most important among these are friction between the

rollers, possibly causing some stretching of the mid surface of the shell, and the use of a uniaxial tension test to characterize biaxial strain hardening behaviour involving both tensile and compressive strains.

However, the excellent agreement between our predictions and experimental results suggests that these effects are indeed small, at least for the cases considered.

Acknowledgements

We thank Mr Andrew Daton-Lovett for introducing us to the challenges of bistable shell structures, and Professor C.R. Calladine for first showing us a bistable toy bracelet. This research has been sponsored by EPSRC (research grant GR/M72852/01) and supported by Rolatube Technology Ltd. SDG acknowledges support from the Leverhulme Trust.

References

Calladine, C.R. (1983). Theory of Shell Structures, Cambridge University Press, Cambridge.

Crisfield, M.A., 1991. *Non-linear finite element analysis of solids and structures. Volume 1: essentials*, John Wiley and Sons, Chichester.

Daton-Lovett, A., 1996. An extendible member. *Patent Cooperation Treaty Application*, PCT/GB97/00839.

Galletly, D.A. and Guest, S.D., 2003a. Bistable composite slit tubes I: A beam model. In preparation.

Galletly, D.A. and Guest, S.D., 2003b. Bistable composite slit tubes II: A shell model. In preparation.

Guest, S.D. and Pellegrino, S., 2003. Simple analytical models for bistable cylindrical shells. In preparation.

Hyer, M.W., 1981a. Some observations on the cured shape of thin unsymmetric laminates. *J. Composite Materials*, **15**, 175-194.

Hyer, M.W., 1981b. Calculations of the room-temperature shapes of unsymmetric laminates. *J. Composite Materials*, **15**, 296-310.

Iqbal, K. and Pellegrino, S., 2000. Bi-stable composite shells. In: *Proc. 41st AIAA ASME/ ASCE/AHS/ASC Structures, Structural Dynamics and Materials*

Conference, 3-6 April 2000, Atlanta, GA, AIAA 2000-1385.

Iqbal, K., Pellegrino, S. and Daton-Lovett, A., 2000. Bi-stable composite slit tubes. In: *Proc. IUTAM-IASS Symposium on Deployable Structures: Theory and Applications*, (Edited by S. Pellegrino and S. D. Guest), pp 153-162. Kluwer Academic Publishers, Dordrecht.

Lubliner, J., 1990. *Plasticity Theory*, Macmillan Publishing Company, New York.

MacNaughton, J.D., Weyman, H.N. and Groskopfs, E., 1967. The Bi-stem - A new technique in unfurlable structures. In: *Proc. Second Aerospace Mechanisms Symposium*, University of Santa Clara, California pp 139-145. NASA JPL TM33-355.

Rimrott, F.P.J., 1965. Storable tubular extendible member: a unique machine element. *Machine Design*, **37**, 156-163.

Timoshenko, S.P. and Woinowsky-Krieger, S., 1959. em Theory of plates and shells, McGraw-Hill Kogakusha, Tokyo.

The MathWorks Inc., 2002. Matlab 6.5. Natick, MA.

Table 1: Properties of Beryllium-Copper in tension (test cases 3 and 4)

Linear properties		Non-linear properties	
		ε^y	σ^y (N/mm^2)
		0	0
Young's modulus	$E = 1.30 \times 10^5$ N/mm^2	0.0050	650
		0.0062	780
Yield stress	$\sigma_0^y = 650$ N/mm^2	0.0075	883
		0.0088	949
Poisson's ratio	$\nu = 0.3$	0.0105	1003
		0.0125	1043
		0.0145	1071
		0.0168	1096
		0.0200	1123

Table 2: Properties of Beryllium-Copper specimens

Test case	Dimensions (mm^2)	t (mm)	Radius ($1/\kappa_{0y}$) (mm)
1, 2	50×50	0.1	10
3, 4			14
5, 6			19

Table 3: Comparison between tests and theoretical predictions.

Test case		$1/\kappa_{2x}$ (mm)	$1/\kappa_{3x}$ (mm)	$1/\kappa_{5y}$ (mm)	$1/\kappa_{3x'}$ (mm)
1	Test	-3.2	-15	18	-18
	Analysis		-19	20	-19
2	Test	-4	-34	15	-45*
	Analysis		-43	15	-44
3	Test	-3.2	-11	30	-15
	Analysis		-13	44	-15
4	Test	-4	-21	23	-24
	Analysis		-26	24	-26
5	Test	-3.2	-18	36	-22
	Analysis		-19	38	-19
6	Test	-4	-46	26	-60
	Analysis		-48	26	-49

* Almost unstable.

Figure 1: Steel tape measure (*Ca.* 1950). Note that the transverse curvature of the extended tape and the longitudinal curvature of the coiled tape are in the same sense.

(a) (b) (c)

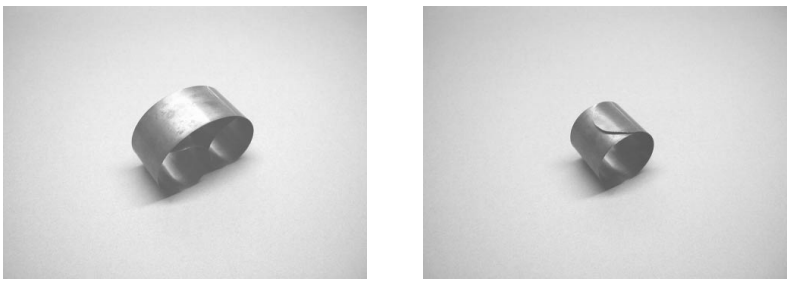

(d) (e)

Figure 2: Transition from extended to rolled-up configuration of a bistable prestressed shell; the configurations (b-d) are unstable.

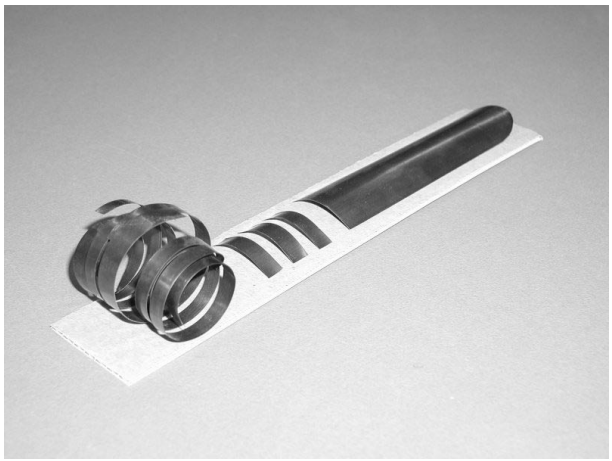

Figure 3: Sliced-up shell.

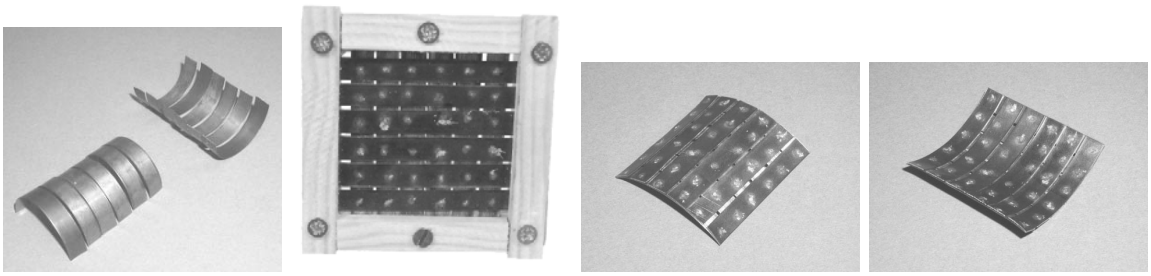

(a) (b) (c) (d)

Figure 4: Bi-stable structure made of half-circular strips.

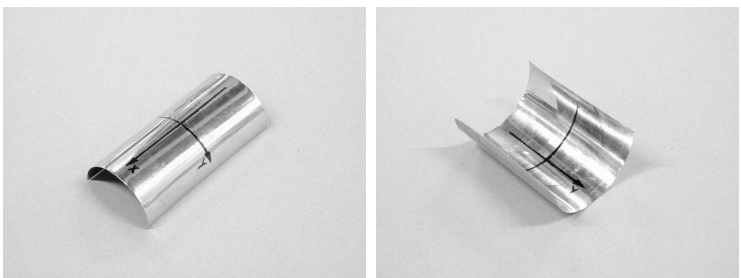

Figure 5: Bi-stable shell made of Beryllium-Copper.

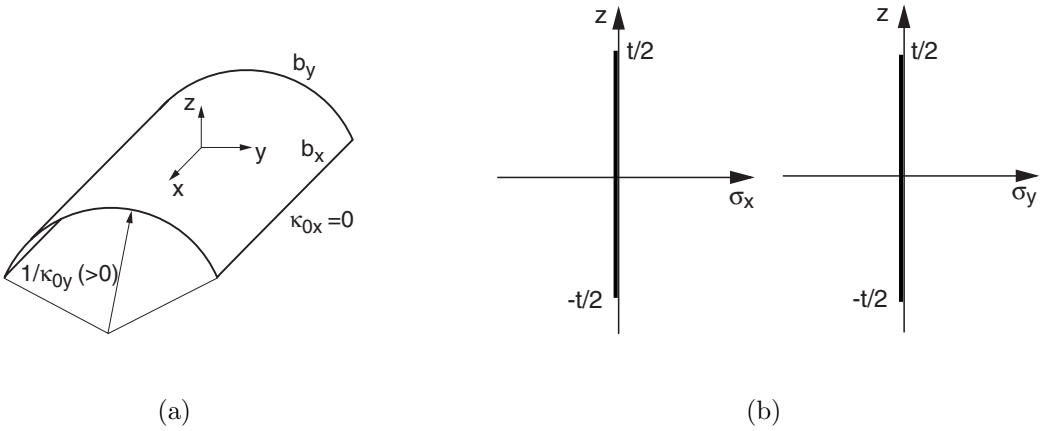

(a) (b)

Figure 6: Initial configuration (Step 0).

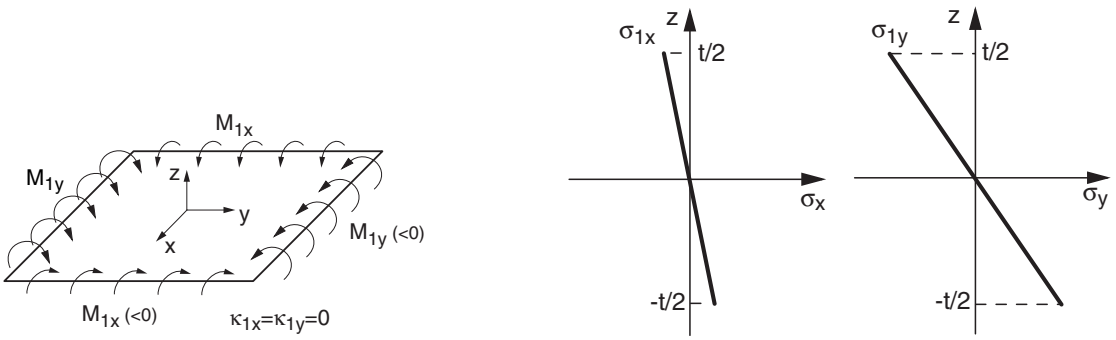

(a) (b)

Figure 7: Flattening the shell (Step 1).

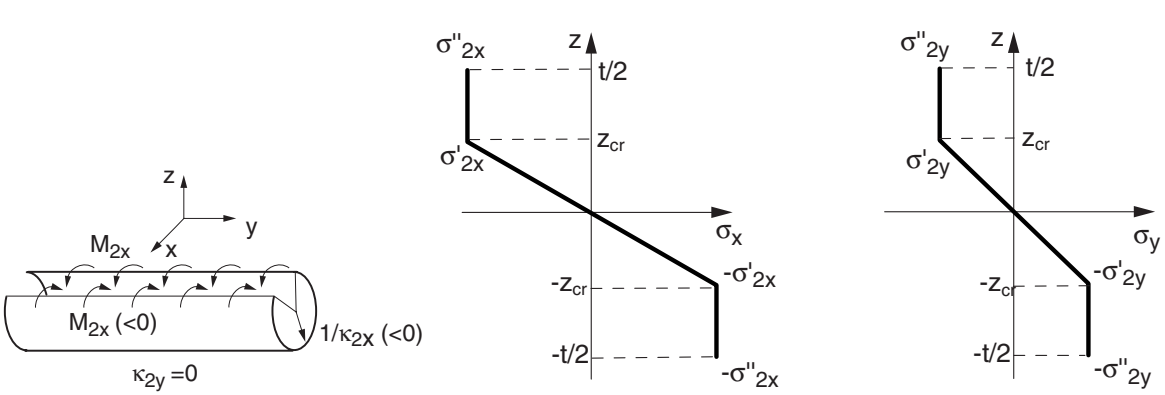

(a) (b)

Figure 8: Yielding the shell (Step 2).

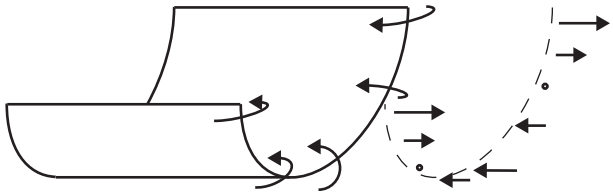

Figure 9: Bending stresses in equilibrium with membrane stresses.

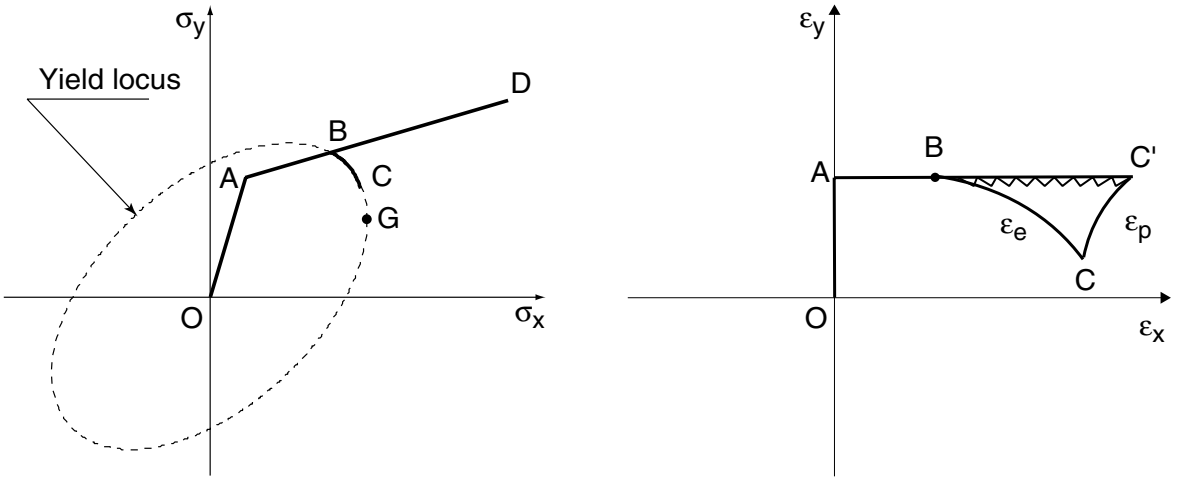

(a) (b)

Figure 10: Stress (a) and strain (b) trajectories for a point at $z = -t/2$, during Steps 1 and 2.

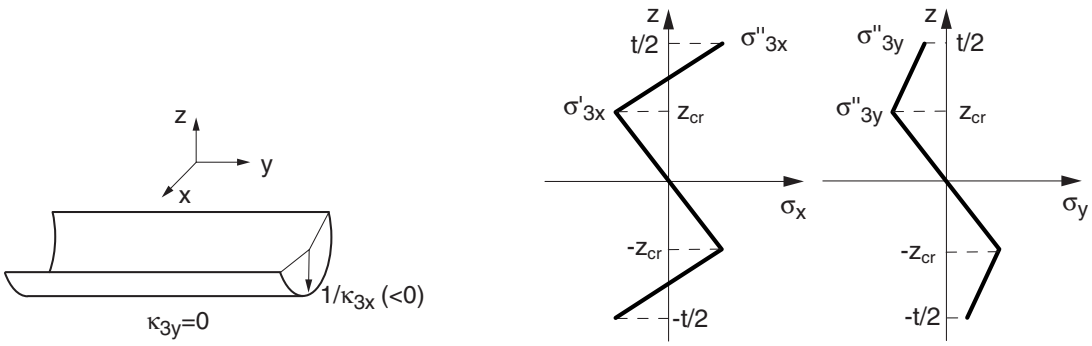

(a) (b)

Figure 11: Unloading the shell (Step 3).

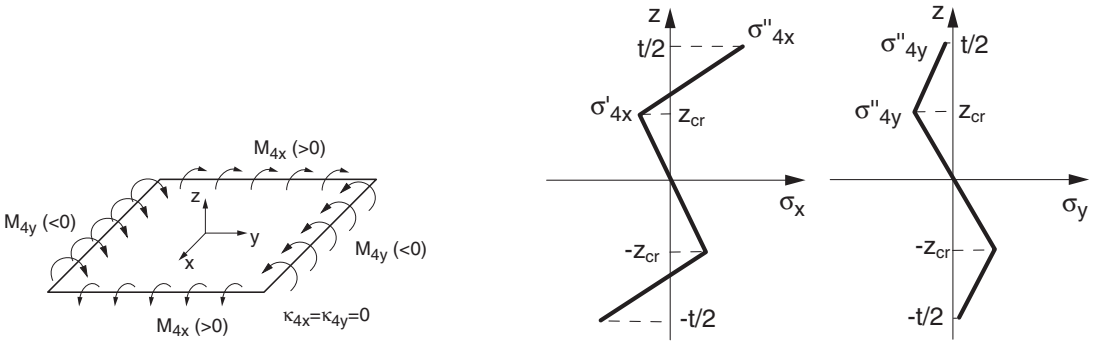

(a) (b)

Figure 12: Flattening the shell before flipping it (Step 4).

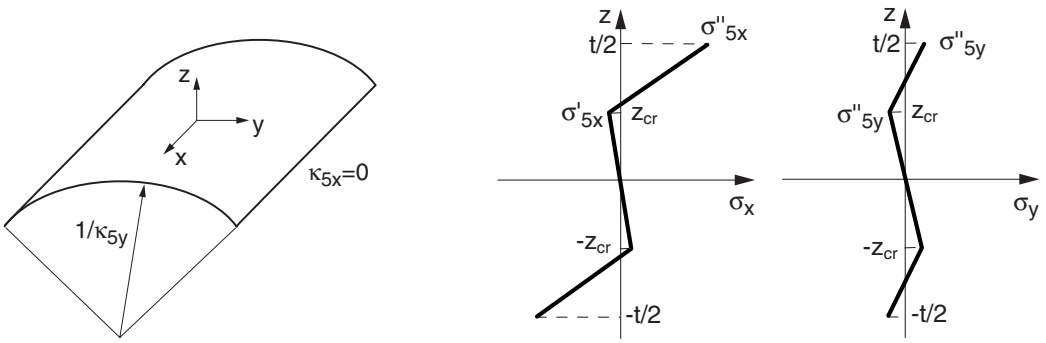

(a) (b)

Figure 13: Flipping the shell (Step 5).

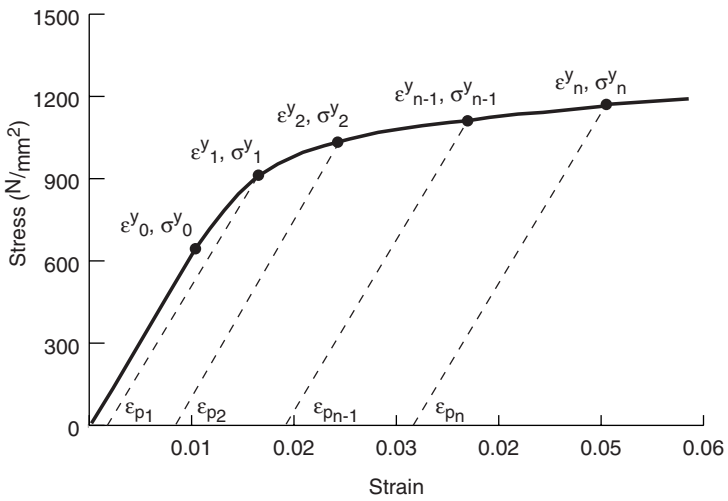

Figure 14: Uniaxial stress-strain relationship for test cases 3 and 4.

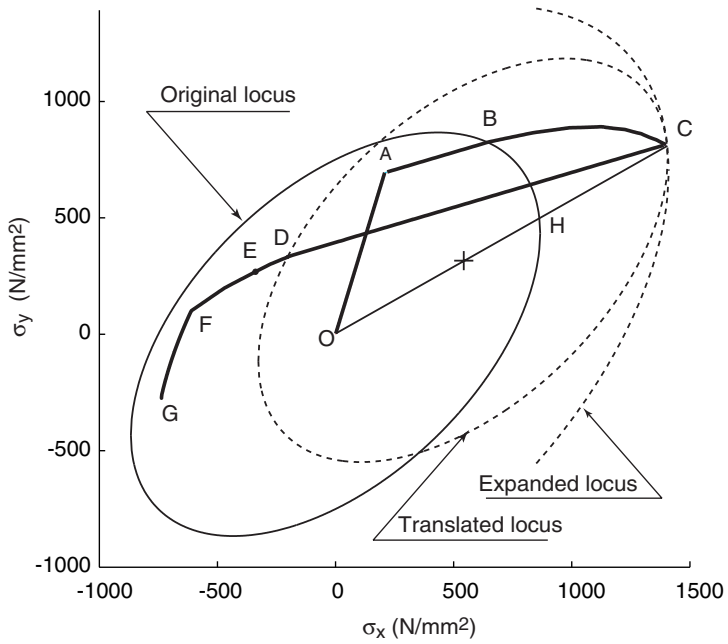

Figure 15: Yield locus and stress path for a point lying on the outer surface of the shell.

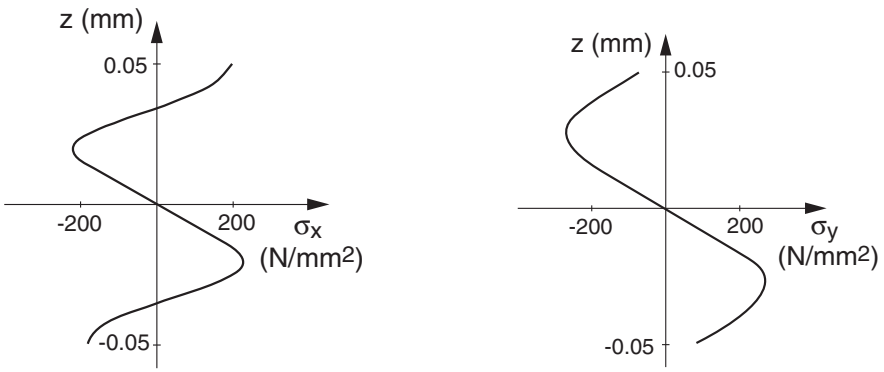

(a) (b)

Figure 16: Predicted stress distribution in test case 3, after forming.

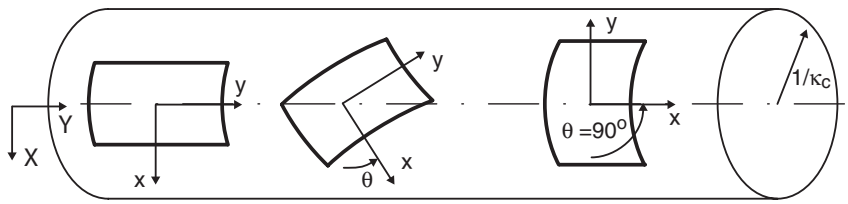

Figure 17: Rotation (twisting) of a curved shell on a cylindrical surface.

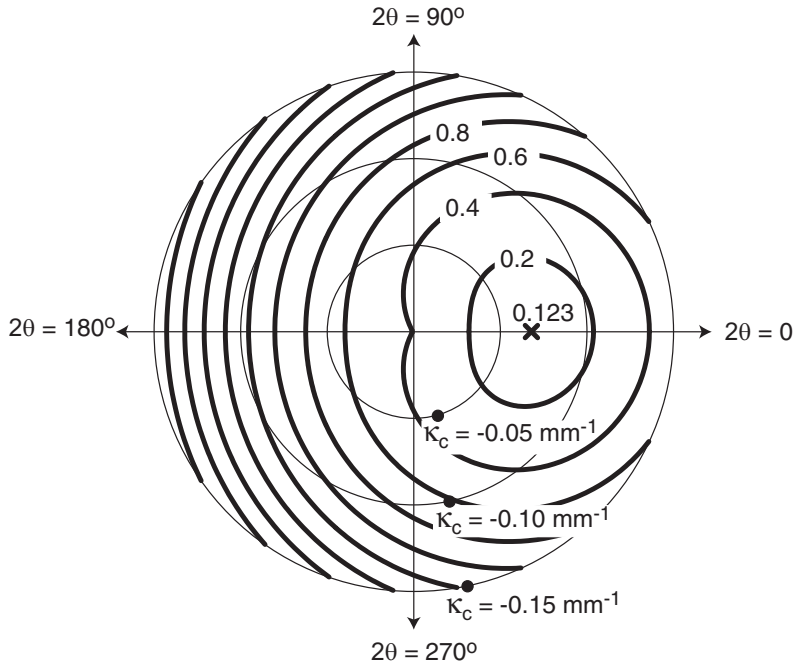

(a) Negative curvatures

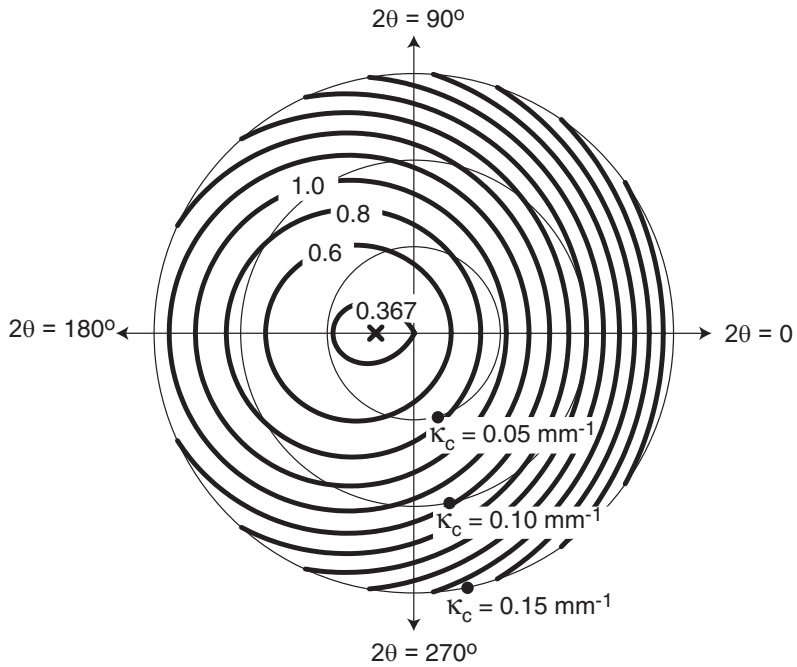

(b) Positive curvatures

Figure 18: Contour plots, at intervals of 0.2 N/mm, of total strain energy per unit area (units N/mm) for test case 3, showing two local minima and hence two stable configurations.